Vertical muon intensity measured with MACRO at the Gran Sasso laboratory

M. Ambrosio,[12] R. Antolini,[7] G. Auriemma,[14,*] R. Baker,[11] A. Baldini,[13] G. C. Barbarino,[12] B. C. Barish,[4] G. Battistoni,[6,†] R. Bellotti,[1] C. Bemporad,[13] P. Bernardini,[10] H. Bilokon,[6] V. Bisi,[16] C. Bloise,[6] C. Bower,[8] S. Bussino,[14] F. Cafagna,[1] M. Calicchio,[1] D. Campana,[12] M. Carboni,[6] M. Castellano,[1] S. Cecchini,[2,‡] F. Cei,[13,§] P. Celio,[14] V. Chiarella,[6] A. Corona,[14] S. Coutu,[11] G. De Cataldo,[1] H. Dekhissi,[2,‖] C. De Marzo,[1] I. De Mitri,[9] M. De Vincenzi,[14,¶] A. Di Credico,[7,14] O. Erriquez,[1] C. Favuzzi,[1] C. Forti,[6] P. Fusco,[1] G. Giacomelli,[2] G. Giannini,[13,**] N. Giglietto,[1] M. Grassi,[13] A. Grillo,[7] F. Guarino,[12] P. Guarnaccia,[1] C. Gustavino,[7] A. Habig,[8] K. Hanson,[11] A. Hawthorne,[8] R. Heinz,[8] J. T. Hong,[3] E. Iarocci,[6,††] E. Katsavounidis,[4] E. Kearns,[3] S. Kyriazopoulou,[4] E. Lamanna,[14] C. Lane,[5] D. S. Levin,[11] P. Lipari,[14] R. Liu,[4] N. P. Longley,[4] M. J. Longo,[11] Y. Lu,[15] G. Ludlam,[3] G. Mancarella,[10] G. Mandrioli,[2] A. Margiotta-Neri,[2] A. Marini,[6] D. Martello,[10] A. Marzari-Chiesa,[16] M. N. Mazziotta,[1] D. G. Michael,[4] S. Mikheyev,[7,‡‡] L. Miller,[8] M. Mittelbrunn,[5] P. Monacelli,[9] T. Montaruli,[1] M. Monteno,[16] S. Mufson,[8] J. Musser,[8] D. Nicoló,[13,§] R. Nolty,[4] C. Okada,[3] C. Orth,[3] G. Osteria,[12] O. Palamara,[10] S. Parlati,[7] V. Patera,[6,††] L. Patrizii,[2] R. Pazzi,[13] C. W. Peck,[4] S. Petrera,[10] N. D. Pignatano,[4] P. Pistilli,[10] V. Popa,[2,§§] A. Rainó,[1] J. Reynoldson,[7] F. Ronga,[6] A. Sanzgiri,[15] F. Sartogo,[14] C. Satriano,[14,*] L. Satta,[6,††] E. Scapparone,[2] K. Scholberg,[4] A. Sciubba,[6,††] P. Serra-Lugaresi,[2] M. Severi,[14] M. Sitta,[16] P. Spinelli,[1] M. Spinetti,[6] M. Spurio,[2] R. Steinberg,[5] J. L. Stone,[3] L. R. Sulak,[3] A. Surdo,[10] G. Tarlé,[11] F. Tassoni,[14] V. Togo,[2] V. Valente,[6] C. W. Walter,[4] and R. Webb[15]

(MACRO Collaboration)

[1] *Dipartimento di Fisica dell'Università di Bari and Istituto Nazionale di Fisica Nucleare, 70126 Bari, Italy*
[2] *Dipartimento di Fisica dell'Università di Bologna and Istituto Nazionale di Fisica Nucleare, 40126 Bologna, Italy*
[3] *Physics Department, Boston University, Boston, Massachusetts 02215,*
[4] *California Institute of Technology, Pasadena, California 91125,*
[5] *Department of Physics, Drexel University, Philadelphia, Pennsylvania 19104*
[6] *Laboratori Nazionali di Frascati dell'Istituto Nazionale di Fisica Nucleare, 00044 Frascati (Roma), Italy*
[7] *Laboratori Nazionali del Gran Sasso dell'Istituto Nazionale di Fisica Nucleare, 67010 Assergi (L'Aquila), Italy*
[8] *Departments of Physics and of Astronomy, Indiana University, Bloomington, Indiana 47405*
[9] *Dipartimento di Fisica dell'Università dell'Aquila and Istituto Nazionale di Fisica Nucleare, 67100 L'Aquila, Italy*
[10] *Dipartimento di Fisica dell'Università di Lecce and Istituto Nazionale di Fisica Nucleare, 73100 Lecce, Italy*
[11] *Department of Physics, University of Michigan, Ann Arbor, Michigan 48109*
[12] *Dipartimento di Fisica dell'Università di Napoli and Istituto Nazionale di Fisica Nucleare, 80125 Napoli, Italy*
[13] *Dipartimento di Fisica dell'Università di Pisa and Istituto Nazionale di Fisica Nucleare, 56010 Pisa, Italy*
[14] *Dipartimento di Fisica dell'Università di Roma "La Sapienza" and Istituto Nazionale di Fisica Nucleare, 00185 Roma, Italy*
[15] *Physics Department, Texas A&M University, College Station, Texas 77843*
[16] *Dipartimento di Fisica Sperimentale dell'Università di Torino and Istituto Nazionale di Fisica Nucleare, 10125 Torino, Italy*

The vertical underground muon intensity has been measured in the slant depth range 3200–7000 hg cm^{-2} (standard rock) with the completed lower part of the MACRO detector at the Gran Sasso

*Also at Università della Basilicata, 85100 Potenza, Italy.
†Also at INFN Milano, 20133 Milano, Italy.
‡Also at Istituto TESRE/CNR, 40129 Bologna, Italy.
§Also at Scuola Normale Superiore di Pisa, 56010 Pisa, Italy.
‖Also at Faculty of Sciences, University Mohamed I, B.P. 424 Oujda, Morocco.
¶Also at Dipartimento di Fisica, Università di Roma III, Roma, Italy.

**Also at Università di Trieste and INFN, 34100 Trieste, Italy.
††Also at Dipartimento di Energetica, Università di Roma, 00185 Roma, Italy.
‡‡Also at Institute for Nuclear Research, Russian Academy of Science, 117312 Moscow, Russia.
§§Also at Institute for Atomic Physics, 76900 Bucharest, Romania.

laboratory, using a large sample of data. These observations are used to compute the surface muon flux and the primary "all-nucleon" spectrum. An analysis of systematic uncertainties introduced by the interaction models in the atmosphere and the underground propagation of muons is presented. A comparison of our results with published data is also presented.

PACS number(s): 13.85.Tp, 96.40.Tv

I. INTRODUCTION

In this work we present a new measurement of the inclusive flux of underground muons performed with the Monopole, Astrophysics, and Cosmic Ray Observatory (MACRO) detector running at the Gran Sasso National Laboratory in central Italy.

Muons detected in deep underground detectors can provide information on the spectrum and composition of primary cosmic rays [1] in the energy range $E_0 \simeq 10^{14}$–10^{16} eV. The most sensitive measurements are obtained by considering the frequency of events as a function of the muon multiplicity [2]. For this purpose it is necessary to have detectors with geometrical dimensions large with respect to the average separation [3] of underground muons. The sensitivity of the measurements is improved if the measurement of the muon multiplicity underground is accompanied by the coincident measurement of other properties of the primary particle induced shower [4]. In the measurement of the inclusive muon intensity that is discussed here, one considers the total flux of muons observed underground for different slanted depths and different zenith angles, summing over all muon multiplicities, without considering correlations with other measurements of the primary particle shower. In this way some amount of information is lost; however, this measurement is interesting for several reasons: The complications of determining the detector acceptance for multiple muon events [3] are absent, the inclusive muon flux has been measured before with smaller detectors, and our results can be compared to these earlier measurements. The inclusive muon flux can be related to the inclusive flux of primary nucleons, i.e., the flux of nucleons obtained summing over all primary masses. In fact the composition of the primary cosmic rays is important in determining the multiplicity distribution of the underground muon events, but has a negligible effect on the inclusive muon flux.

The determination of the "all-nucleon" flux obtained with this technique is competitive with measurements obtained with direct [5] and indirect [6] methods that are limited, respectively, by statistical and systematic uncertainties. On the other hand a comparison of the "all-nucleon" primary flux determined from the underground muon intensity with the results obtained with other methods is a sensitive test of the models of muon production in hadronic showers that are used to study the cosmic ray composition [2].

We shall discuss measurements of the underground muon flux in the range of depth $3200 \leq h \leq 7000$ hg cm^{-2}. The minimum depth is determined by the location of the underground laboratory where the MACRO detector is located. The region of very large depths, including the region where neutrino interactions in the

vicinity of the detector become the dominant source of muons, will be discussed in a future paper.

The measured muon flux in the slant depth region considered corresponds to the muon spectrum at the surface in the energy range 1–20 TeV. The corresponding all-nucleon primary flux is in the energy range 2–200 TeV.

Results on the underground muon intensity obtained by the MACRO Collaboration with a limited portion of the detector in operation were presented in [7]. In the present work we discuss a data sample 10 times larger and give a more complete discussion of the systematic effects that dominate the uncertainty in the measurement.

The paper is organized as follows: in Sec. II we briefly discuss the detector and the data selection criteria used; in Sec. III we present our determination of the underground muon intensity; in Sec. IV we use the results to estimate the all-nucleon primary spectrum considering uncertainties in the modeling of muon production; in Sec. V we discuss the sea-level muon spectrum ($E_\mu \geq 1$ TeV) implied by our measurement and compare the results with earlier measurements [8, 9].

II. DETECTOR AND DATA SELECTION

The present analysis was carried out on data collected with the completed lower part of the MACRO detector, with an acceptance of $S\Omega \simeq 3100$ m^2 sr for atmospheric muons. The lower structure consists of six nearly identical units, called supermodules, of 12 m × 12 m × 4.8 m. Each supermodule, described in detail elsewhere [10], consists of ten horizontal planes of streamer tubes. The eight innermost planes are separated by seven layers, each of $\simeq 60$ g cm^{-2} absorbers of low activity Gran Sasso rock. The two outermost planes are separated by two 19 cm layers of liquid scintillators. The lateral walls consist of stacked tanks of liquid scintillator, 25 cm thick, sandwiched between six vertical streamer tubes planes.

All streamer tube wires are read out, providing the X coordinate on the horizontal planes and the Z coordinate on the vertical planes. On the horizontal planes the second coordinate D is obtained by reading the pulses induced on horizontal aluminum strips oriented at 26.5° with respect to the streamer tubes axis, to allow stereoscopic reconstruction. Muon tracks are thus reconstructed with an angular resolution of 0.2°. The systematic uncertainty in the zenith angle reconstruction has been carefully checked for muon astronomy measurements and is less than 0.25° [11]. This resolution is negligible compared to the average multiple scattering angle of 0.8° for muons crossing the overburden rock. This value is consistent with the angular differences measured between muons belonging to the same event detected in MACRO.

Data were collected starting in July 1991, after the completion of the lower part of MACRO while the upper part was still under construction; use was made of only the streamer tube system of the completed lower part. The hardware trigger was defined by either six streamer tube planes fired anywhere, or five consecutive horizontal planes, excluding the first and the last ones. A muon track is reconstructed if at least four horizontal planes are recorded, both in the wire and strip views. The data runs were then selected as follows: Runs were accepted if they had ≥ 4 h duration, and had a dead time smaller than 1% and a counting rate per hour per supermodule inside a range of $\pm 3\sigma$ around the mean value simultaneously for all the six supermodules. These requirements assure a full and uniform acceptance of the apparatus. After these cuts, we have 3.91×10^6 muons for a live time of 4228 h. These statistics are more than one order of magnitude larger than those reported in [7]. The large statistics allows us to study the Gran Sasso rock systematics and to reject angular regions where the muon intensities are not compatible with the measured average intensities of the regions with the same nominal rock thickness, as described in the Appendix.

III. VERTICAL MUON INTENSITY

The total data sample (single and multiple muons) is used to determine the bin-by-bin muon intensity $I_\mu(h, \theta, \phi)$ as

$$I_\mu(h, \theta, \phi) = \left(\frac{1}{\Delta T}\right) \frac{\Sigma_i N_i m_i}{\Sigma_j \Delta\Omega_j A_j \epsilon_j} , \qquad (1)$$

where ΔT is the live time, N_i is the number of observed events of muon multiplicity m_i in the angular bin $\Delta\Omega_j$ of slant depth h (taken from the military topographical map of the mountain, as described in the Appendix), A_j is the geometric detector projected area for that bin, ϵ_j is the combined trigger and reconstruction efficiency, θ is the muon zenith angle, and ϕ is the azimuth angle. The data are binned with $\Delta\theta = 1°$, $\Delta\phi = 2°$.

The projected area $A_j(\theta, \phi)$ and the detector tracking efficiency $\epsilon_j(\theta, \phi)$ were calculated with accuracies better than 1% from a Monte Carlo program, based on GEANT [12] to produce simulated data which were processed through the same off-line program chain used for the real data. All sources of inefficiencies (detector, electronics, and trigger) are included in the Monte Carlo program. The product $A_j \times \epsilon_j$ is shown in Fig. 1 as a function of the polar and azimuthal angles.

For each bin the Gran Sasso rock thickness (in meters) was converted to standard rock slant depth (in $\mathrm{hg\,cm^{-2}}$) using the Gran Sasso rock parameters listed in Table IV, below, and a conversion formula described in Ref. [13].

In order to compare our results with those of other experiments, we calculated the vertical muon intensity using the well-known $\sec(\theta)$ angular dependence (valid up to 60° [1]):

$$I_\mu^v(h, \theta, \phi) = \left(\frac{1}{\Delta T}\right) \frac{\Sigma_i N_i m_i}{\Sigma_j \Delta\Omega_j A_j \epsilon_j / \cos\theta_j} . \qquad (2)$$
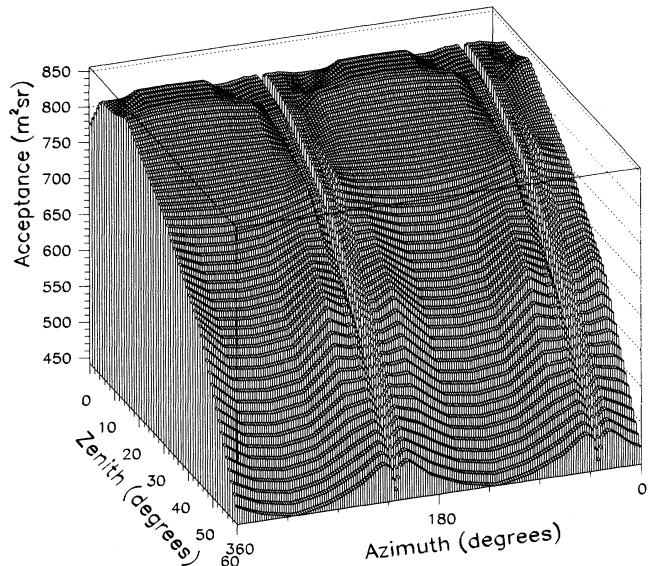

FIG. 1. Projected area A_j times efficiency ϵ_j of the detector versus geographical coordinates. The polar angle extends up to 60°.

We have considered 54 bins of equal slant depth h, of width $\Delta h = 50$ $\mathrm{hg\,cm^{-2}}$ for the range $3200 < h < 4750$ $\mathrm{hg\,cm^{-2}}$; for the range $4750 < h < 6950$ $\mathrm{hg\,cm^{-2}}$ we have used bins of $\Delta h = 100$ $\mathrm{hg\,cm^{-2}}$. The measured underground vertical muon intensity as a function of the slant depth h, for the zenith range 0°–60°, is given in Table I and is shown in Fig. 2. Each point is the mean value of the $I_\mu^v(h, \theta, \phi)$ distribution at fixed slant depth h.

We explored the effects of the main sources of systematics. The use of an average rock density (estimated using the results of the bore hole surveys of the mountain) instead of a function depending on the zenithal and azimuthal angles contributes an uncertainty of about $\pm 1.5\%$ to the rock thickness, corresponding to $\pm 5\%$ on the muon intensity at 3200 $\mathrm{hg\,cm^{-2}}$. A further 5% contribution to the absolute scale of the muon intensity comes from the assumption of a homogeneous mountain instead of a layered structure as modeled in Ref. [14] and described in [15]. The total systematic uncertainty is estimated at $\pm 8\%$.

In the range 3200–7000 $\mathrm{hg\,cm^{-2}}$ our data are well fitted by the three-parameter empirical formula

$$I_\mu(h) = A \left(\frac{h_0}{h}\right)^\alpha e^{-\frac{h}{h_0}} , \qquad (3)$$

with $A = (1.96 \pm 0.03) \times 10^{-6}$ $\mathrm{cm^{-2}\,s^{-1}\,sr^{-1}}$, $\alpha = 1.10 \pm 0.01$, and $h_0 = (972 \pm 3)$ $\mathrm{hg\,cm^{-2}}$ with a $\chi^2/N_{\mathrm{DF}} = 65/51$. Using the Frejus function [16]

$$I_\mu(h) = B \left(\frac{h_1}{h}\right)^2 e^{-\frac{h}{h_1}} , \qquad (4)$$

we obtain $B = (1.81 \pm 0.06) \times 10^{-6}$ $\mathrm{cm^{-2}\,s^{-1}\,sr^{-1}}$ and $h_1 = (1231 \pm 1)$ $\mathrm{hg\,cm^{-2}}$ with a $\chi^2/N_{\mathrm{DF}} = 76/52$. The errors quoted for the fitted parameters include statisti-

TABLE I. Measured vertical muon underground intensity $I_\mu(h)$ (muons cm^{-2} s^{-1} sr^{-1}) versus slant depth of standard rock (hg cm^{-2}). The quoted errors include statistical uncertainties and systematic uncertainties for the topographical map. The additional estimated systematic scale uncertainty is $\pm 8\%$; see text.

Depth	$I(h) \pm \Delta I(h)$	Depth	$I(h) \pm \Delta I(h)$
3200	$(2.00 \pm 0.01) \times 10^{-8}$	4550	$(3.29 \pm 0.07) \times 10^{-9}$
3250	$(1.85 \pm 0.01) \times 10^{-8}$	4600	$(3.05 \pm 0.07) \times 10^{-9}$
3300	$(1.73 \pm 0.01) \times 10^{-8}$	4650	$(2.92 \pm 0.04) \times 10^{-9}$
3350	$(1.59 \pm 0.01) \times 10^{-8}$	4700	$(2.72 \pm 0.06) \times 10^{-9}$
3400	$(1.48 \pm 0.01) \times 10^{-8}$	4762	$(2.61 \pm 0.04) \times 10^{-9}$
3450	$(1.39 \pm 0.01) \times 10^{-8}$	4850	$(2.32 \pm 0.06) \times 10^{-9}$
3500	$(1.30 \pm 0.01) \times 10^{-8}$	4950	$(2.02 \pm 0.06) \times 10^{-9}$
3550	$(1.215 \pm 0.008) \times 10^{-8}$	5050	$(1.86 \pm 0.03) \times 10^{-9}$
3600	$(1.144 \pm 0.008) \times 10^{-8}$	5150	$(1.60 \pm 0.04) \times 10^{-9}$
3650	$(1.058 \pm 0.007) \times 10^{-8}$	5250	$(1.40 \pm 0.02) \times 10^{-9}$
3700	$(1.000 \pm 0.007) \times 10^{-8}$	5350	$(1.28 \pm 0.04) \times 10^{-9}$
3750	$(9.44 \pm 0.07) \times 10^{-9}$	5450	$(1.05 \pm 0.03) \times 10^{-9}$
3800	$(8.85 \pm 0.06) \times 10^{-9}$	5550	$(9.6 \pm 0.2) \times 10^{-10}$
3850	$(8.23 \pm 0.06) \times 10^{-9}$	5650	$(8.7 \pm 0.2) \times 10^{-10}$
3900	$(7.73 \pm 0.07) \times 10^{-9}$	5750	$(7.5 \pm 0.1) \times 10^{-10}$
3950	$(7.20 \pm 0.07) \times 10^{-9}$	5850	$(6.8 \pm 0.2) \times 10^{-10}$
4000	$(6.75 \pm 0.06) \times 10^{-9}$	5950	$(5.8 \pm 0.5) \times 10^{-10}$
4050	$(6.37 \pm 0.06) \times 10^{-9}$	6050	$(5.2 \pm 0.3) \times 10^{-10}$
4100	$(5.88 \pm 0.06) \times 10^{-9}$	6150	$(4.6 \pm 0.2) \times 10^{-10}$
4150	$(5.49 \pm 0.06) \times 10^{-9}$	6250	$(4.3 \pm 0.1) \times 10^{-10}$
4200	$(5.15 \pm 0.05) \times 10^{-9}$	6350	$(3.6 \pm 0.7) \times 10^{-10}$
4250	$(4.82 \pm 0.06) \times 10^{-9}$	6450	$(3.2 \pm 0.4) \times 10^{-10}$
4300	$(4.51 \pm 0.05) \times 10^{-9}$	6550	$(2.7 \pm 0.3) \times 10^{-10}$
4350	$(4.21 \pm 0.07) \times 10^{-9}$	6650	$(2.7 \pm 0.5) \times 10^{-10}$
4400	$(3.94 \pm 0.07) \times 10^{-9}$	6750	$(2.2 \pm 0.3) \times 10^{-10}$
4450	$(3.69 \pm 0.09) \times 10^{-9}$	6850	$(2.2 \pm 0.3) \times 10^{-10}$
4500	$(3.46 \pm 0.03) \times 10^{-9}$	6950	$(2.0 \pm 0.3) \times 10^{-10}$

cal uncertainties and point-to-point uncertainties in the Gran Sasso map.

Figure 3 shows the behavior of the intensity as a function of $\sec(\theta)$ at fixed depths. In Fig. 3(a) the data were binned in four depth regions of rock and in Fig. 3(b) the experimental points are scaled to the central slant depth value $h = 5400$ hg cm^{-2}, using the empirical relation described in item (b) of Ref. [6]. The quoted errors include statistical and point-to-point uncertainties; the global systematic uncertainties related to the mountain knowledge are not included. The linear behavior of the data is an *a posteriori* confirmation of the angular dependence of the underground muon intensity.

In Fig. 4(a) our data are compared with the world data in the range 1000–17 000 hg cm^{-2}; Fig. 4(b) is a blowup of the slant depth region relevant to our present results. Our data agree, within their combined statistical and systematic uncertainties, with the data of other experiments. In Fig. 4(b) our fit is compared to previous fits of other experiments and to the Crouch compilation presented in Ref. [17]. A difference of about 40% is found between MACRO and the Nucleon Stability Experiment (NUSEX), where the data overlap [8]. The Frejus fit [16] differs from ours by about 10–15 %, which corresponds to about one standard deviation of the Frejus fitted parameters. The comparison of our data with the Crouch compilation shows differences of less than 6%. The ob-

served discrepancies with NUSEX might be connected to unknown systematic uncertainties in their rock overburden.

IV. PRIMARY SPECTRUM

In the context of the superposition model, the muon flux at the surface contains information on the "all-
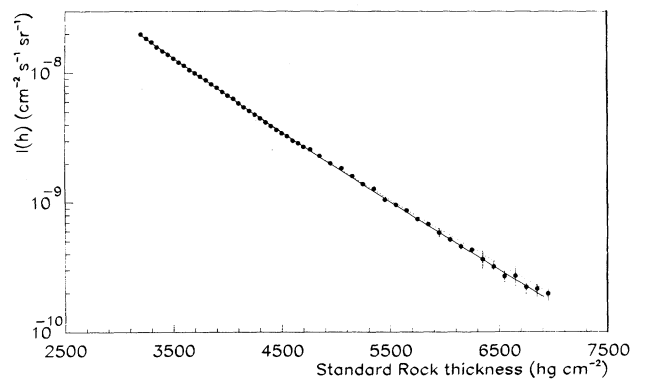

FIG. 2. Measured vertical muon intensity versus standard rock (black points). The dotted and solid lines are the two- and three-parameter fits described in the text.

TABLE II.   Spectrum weighted moments Z_{ij} and atmospheric attenuation lengths Λ_i (in $\mathrm{g\,cm^{-2}}$) for hadrons and primary all-nucleon spectrum coefficients obtained from the three fits described in the text.

| Model | Input | | | Output | |
	Z_{NN}	$Z_{N\pi}$	Z_{NK}	N_0 $(\mathrm{cm^{-2}\,s^{-1}\,sr^{-1}\,GeV^{\gamma_p-1}}A)$	γ_p
Gaisser	0.298	0.079	0.0118	3.4 ± 0.1	2.78 ± 0.04
HEMAS	0.26	0.057	0.0113	5.0 ± 0.1	2.79 ± 0.04
SIBYLL	0.28	0.068	0.0071	4.1 ± 0.1	2.77 ± 0.05
	Λ_N	Λ_π	Λ_K		
All models	120	160	180		

nucleon" primary spectrum $N(E_p)$. In the energy range relevant for the present measurement ($2 < E_p < 200$ TeV/nucleon), the relation between the surface muon flux $\frac{dN_\mu}{dE\,d\Omega}$ and the "all-nucleon" primary spectrum $N(E_p)$ is approximated using the same relations used in Ref. [1] by the formula

$$\frac{dN_\mu}{dE\,d\Omega}$$

$$\simeq N(E_p)\frac{Z_{N\pi}}{1-Z_{NN}}\frac{\left[1-(r_\pi)^{\gamma+1}\right](1-r_\pi)^{-1}(\gamma+1)^{-1}}{1+\frac{B_\pi \cos\theta E}{\epsilon_\pi}},$$

(5)

where

$$B_\pi = \frac{(\gamma+2)}{(\gamma+1)}\frac{1-(r_\pi)^{\gamma+1}}{1-(r_\pi)^{\gamma+2}}\frac{\Lambda_\pi - \Lambda_N}{\Lambda_\pi \ln(\Lambda_\pi/\Lambda_N)},$$
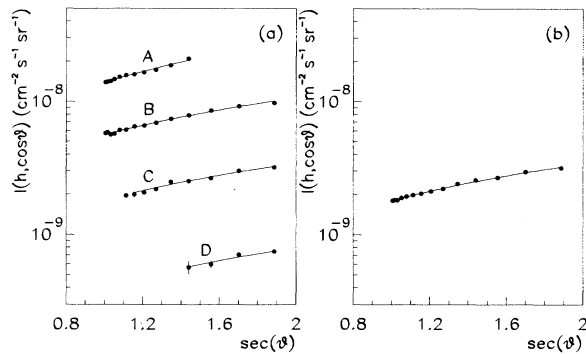
$$r_\pi = \left(\frac{m_\mu}{m_\pi}\right)^2.$$

(6)

Equation (5) is summed over pion and kaon decay channels; B_K and r_K are defined in a similar fashion. The constant $\epsilon_{\pi,K}$ contains the meson lifetimes and depends on the structure of the atmosphere; Z_{ij} are the spectrum averaged moments, which may depend on energy; they contain information on the inclusive distribution as well as on the primary spectrum; Λ_i are the atmospheric attenuation lengths.

Assuming for the "all-nucleon" primary spectrum a simple power dependence

(a)

(b)

FIG. 3.   (a) Muon intensity versus $1/\cos(\theta)$ for four ranges of rock depth: 3150–3750 (A), 3850–4550 (B), 4650–5550 (C), and 5650–6950 $\mathrm{hg\,cm^{-2}}$. (D) The data shown in (a) scaled to $h = 5400$ hg $\mathrm{cm^{-2}}$. The solid lines are linear fits to our data. In the explored angular range (0–60°) and for the energies relevant to our experiment ($E_\mu > 1$ TeV) we do not observe, within the experimental uncertainties, deviations from the conventional $\sec(\theta)$ approximation.
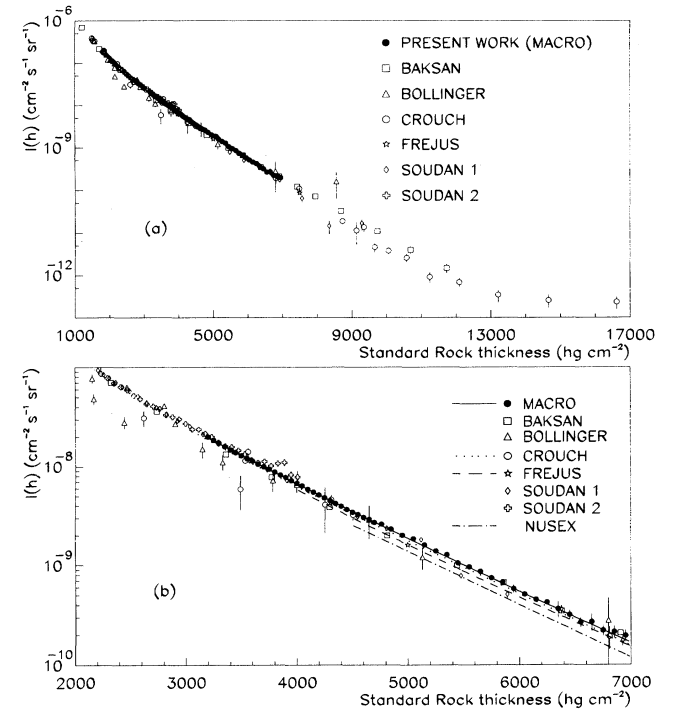
FIG. 4.   Vertical muon intensity versus standard rock. (a) The present MACRO results, the data compiled by Crouch [17], and those obtained by other experiments: BAKSAN [6(g)], Bollinger [6(e)], Frejus [16], and Soudan 1 and Soudan 2 [18]. (b) The depth region covered by our data shown in more detail. The solid line is the fit of our data to Eq. (3), the dotted line is the Crouch fit [17], the dashed line is the Frejus fit, and the dash-dotted line the NUSEX fit.

$$N(E_p) = N_0 E^{-\gamma_p} \tag{7}$$

(well established in the energy range relevant to this measurement), both the spectral index γ_p and the normalization N_0 can be derived from the vertical muon intensity, after the spectrum averaged moments and interaction lengths (as well as details of the atmosphere) are deduced from a Monte Carlo simulation. In the approximation of exact Feynman scaling and a single power spectrum, the spectrum averaged moments and interaction lengths are constant.

We estimated the "all-nucleon" primary spectrum by the least squares method unfolding $N(E_p)$ from the measured underground muon intensity $I_\mu(h)$:

$$I_\mu(h) = \int_0^\infty \frac{dN_\mu}{dE \, d\Omega} P(E, h) dE \ , \tag{8}$$

where h is the rock depth, $\frac{dN_\mu}{dE \, d\Omega}$ is the muon intensity at the surface, and $P(E, h)$ is the survival probability; the integration is performed at constant slant depth values. The survival probabilities were calculated for surface muons with energies in the 1–100 TeV energy range, using a GEANT code especially tuned for the Gran Sasso rock. The code includes a detailed description of muon propagation underground and accounts for fluctuations in muon energy losses [15].

We used different sets of Z_{ij} functions derived from three interaction models: (a) from Ref. [1], where the Z_{ij} are constant as a function of energy since Feynman scaling is assumed to be exact, (b) the HEMAS interaction model [19], and (c) the SIBYLL interaction model [20]. In the latter two cases the Z_{ij} functions exhibit a smooth dependence on primary energy, since scaling violations
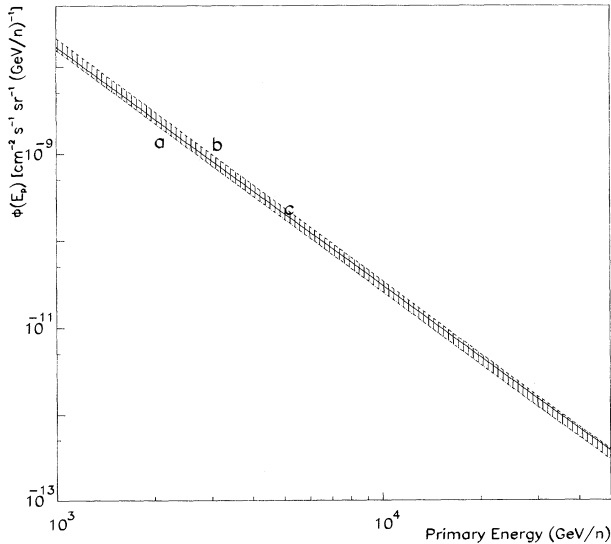

FIG. 6. (a) Differential muon energy flux at the surface, Φ_μ. The solid line is the MACRO fit; it is compared with the available experimental measurements: Allkofer *et al.* [28], Ayre *et al.* [29], Green *et al.* [30], Nandi and Sinha [31], and Rastin [32]. (b) $E_\mu^3 \Phi_\mu(E_\mu)$ is shown as a function of E_μ. The solid line shows the fit to formula (9); the dash-dotted line is from the formula on p. 71 of [1].

are included in the two models. As a reasonable approximation we have chosen the values at 10 TeV/nucleon, since this is the most probable energy of primaries that produce the inclusive muon flux at MACRO depth. We have also made use of constant values for the attenuation lengths given in [1]. The numerical values of these parameters are listed in Table II.

The fit of our data using the three models gives the spectral index γ_p and the normalization factor N_0 quoted in Table II. The correlation coefficient between γ_p and N_0 is 0.975. The errors include both statistical and map resolution uncertainties. Further uncertainties of the order of 5% in N_0 and 3% in γ_p should be considered as discussed in the next section. The spread of the three values gives an estimate of the uncertainties on the primary flux due to the interaction model. Our evaluations are in agreement with the estimates reported in [21]. The values

FIG. 5. "All-nucleon" primary spectrum $\Phi(E_p)$ versus energy E_p. Curves a and b: MACRO values according to the Gaisser (dash-dotted line) and to the HEMAS (dashed line) models (see Table II). Curve c: Average of the direct measurements (solid line) [5, 22]. The dashed area represents the region between the HEMAS and Gaisser models; see Sec. IV.
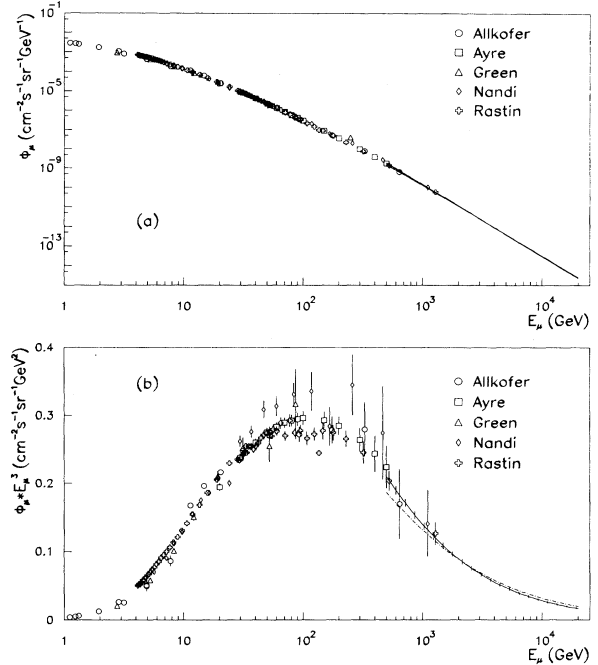
TABLE III. Gran Sasso rock chemical composition [14].

Rock type	Chemical composition	% weight
Dolomite	$CaCO_3$(90%), $MgCO_3$(10%)	50
Dolomite limestone	$CaCO_3$(50%), $MgCO_3$(50%)	29
Flint limestone	$CaCO_3$(72%), SiO_2(8%), Si, Al, K compounds (20%)	8
Karst formation	$CaCO_3$	9
Detritus	$CaCO_3$(49%), $MgCO_3$(1%), Si, Al, K compounds (50 %)	3

TABLE IV.   Gran Sasso rock average parameters. They are very similar to the so-called standard rock for which $A = 22$, $Z = 11$, and $\rho = 2.65$ g cm^{-3}.

$A = 22.87$	$Z = 11.41$	Density $= (2.71 \pm 0.05)$ g cm^{-3}	
Chemical element	Atomic number	Atomic weight	Relative weight
Hydrogen	1	1.008	0.03
Carbon	6	12.011	12.17
Oxygen	8	15.99	50.77
Magnesium	12	24.305	8.32
Aluminum	13	26.981	0.63
Silicon	14	28.085	1.05
Potassium	19	39.098	0.10
Calcium	20	40.078	26.89

corresponding to the Gaisser and the HEMAS models are compared in Fig. 5 with the average of the direct measurements in the energy range 1–50 TeV/nucleon given in [5, 22]. The direct measurements are contained in the dashed region in Fig. 5 which represents the region of our estimate due to the uncertainties of the interaction models. A comment is in order. We notice that the Z functions from HEMAS and SIBYLL, used to reproduce the observed underground muon intensity, produce a reconstructed all-nucleon spectrum higher than that obtained from the average of the existing direct measurements in the range 1–50 TeV/nucleon [5, 22]. This is consistent with the analysis of the muon multiplicity distributions by MACRO [23], where a full simulation using the HEMAS code gave an absolute rate of events 25% lower with respect to the experimental data.

V. MUON FLUX AT THE SURFACE

In order to evaluate the surface muon flux, we follow the same procedure used in Sec. IV, with the parameters of the model described in [1]:

$$\frac{dN_\mu}{dE \, d\Omega} = A_0 E^{-\gamma_\mu} \left(\frac{1}{1 + \frac{1.1 E \cos\theta}{115 \text{ GeV}}} + \frac{0.054}{1 + \frac{1.1 E \cos\theta}{850 \text{ GeV}}} \right) \, . \tag{9}$$

We obtain $A_0 = (0.26 \pm 0.01)$ cm^{-2} s^{-1} sr^{-1} GeV$^{\gamma_\mu-1}$, $\gamma_\mu = 2.78 \pm 0.01$ with a $\chi^2/N_{\text{DF}} = 41/52$. The quoted errors are due to statistics and the map resolution. The fitted parameters are also affected by systematic uncertainties coming from the rock density and the hard energy loss cross sections used to estimate the survival probabilities. The effect of the uncertainty in the rock density produces an estimated uncertainty of 3.5% in A_0 and less than 1% in γ_μ. Because of uncertainties in the bremsstrahlung and photonuclear cross sections [24], the results depend upon the cross sections of the stochastic radiative processes used in GEANT. We used different sets of survival probabilities to test the sensitivity of the fitted parameters to these uncertainties. Using the energy losses of Ref. [25], where a different photoproduction cross section is employed [26], we obtain a variation of $\simeq$ 2% in both A_0 and γ_μ and a $\chi^2/N_{\text{DF}} = 2.9$. We estimate the overall systematic error resulting from rock density and hard energy loss cross sections to be about

5% in A_0 and 3% in γ_μ.

As pointed out in [27], the vertical sea-level muon spectrum is not well known at energies greater than a few hundred GeV; for energies below this range, the statistical and systematic errors of existing experiments are large ($\pm$10–15 %). Hence our determination of the surface muon flux in the energy range $1 < E_p < 20$ TeV provides new information on the high-energy dependence of the sea-level muon spectrum.

In Fig. 6(a) the world data on the surface muon differential flux versus muon energy are presented. The solid line is the fit through our data. In Fig. 6(b) the same data are presented multiplied by E_μ^3. Our fit agrees with the high-energy measurements at sea level. The same figure also shows the differential flux calculation of Ref. [1]. A maximum difference of 10% from our result is observed
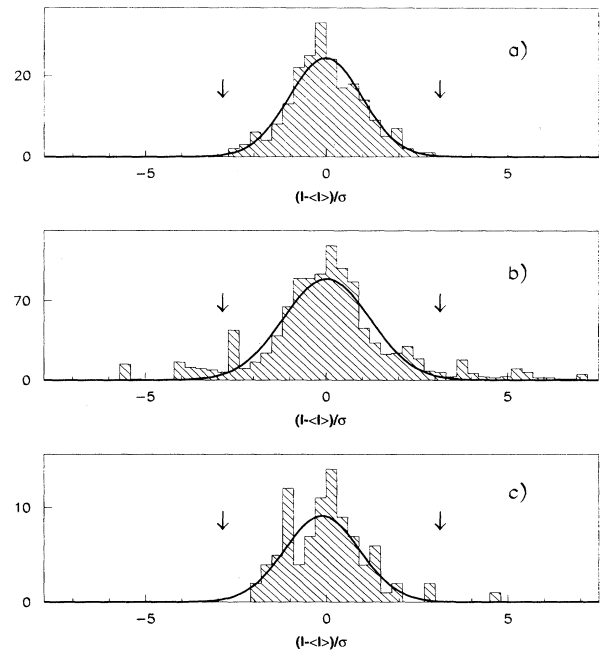

FIG. 7.   Distributions of $[(I(h,\theta,\phi) - \langle I(h,\theta,\phi)\rangle)/\sigma]$ at fixed nominal depth h measured in different angular bins. (a) $h = 3200$ hg cm^{-2}, (b) $h = 3800$ hg cm^{-2}, (c) $h = 5600$ hg cm^{-2}. The solid lines represent Gaussian fits. Points outside $\pm$3 standard deviations have been rejected.

TABLE V. Gran Sasso rock thickness (m) as a function of zenith and azimuth (deg) for the mountain regions where the slant depth of the overburden is known with confidence.

Azimuth (deg.)	Zenith angle (deg)											
	5	10	15	20	25	30	35	40	45	50	55	60
0	1338	1302	1326	1292	1268	1292	1316	1324				
5	1339	1303	1302	1272	1244	1267	1303	1304				
10	1341	1305	1287	1254	1224	1246	1276	1295				
15	1343	1305	1278	1239	1216	1221	1238	1267				
20	1346	1307	1279	1237	1222	1240	1239	1234				
25	1349	1310	1280	1247	1248	1272	1263	1246				
30	1349	1313	1285	1271	1279	1309	1270	1277				
35	1350	1317	1291	1296	1301	1298	1303	1310				
40	1354	1323	1312	1320	1311	1311	1335	1343				
45	1361	1336	1335	1341	1326	1344	1352	1377				
50	1370	1350	1362	1374	1350	1372	1371	1378				
55	1376	1359	1386	1406	1375	1364	1380	1378				
60				1414	1380	1352	1366	1370				
65				1401	1374	1337	1350	1377				
70				1390	1365	1347	1366	1383	1438	1487	1539	1597
75				1388	1371	1371	1384	1419	1471	1516	1562	1659
80				1398	1387	1388	1406	1465	1496	1533	1639	1774
85				1411	1405	1414	1448	1480	1501	1592	1726	1869
90				1420	1426	1446	1481	1495	1547	1674	1804	1908
95				1401	1400	1430	1472	1513	1585	1649	1754	1904
100	1381	1367	1353	1380	1372	1395	1435	1482	1545	1598	1668	1805
105	1377	1358	1328	1352	1361	1353	1401	1427	1486	1557	1615	1760
110	1371	1350	1311	1330	1335	1345	1355	1398	1440	1495		
115	1367	1341	1302	1308	1310	1317	1320	1351	1392	1455		
120	1362	1330	1291	1280	1283	1286	1299	1317	1362	1431		
125	1356	1314	1284	1244	1255	1255	1269	1291	1338	1410		
130	1354	1304	1277	1232	1233	1234	1251	1268	1318	1397		
135	1350	1287	1268	1229	1211	1214	1225	1255	1306	1380		
140	1348	1287	1260	1223	1204	1199	1216	1246	1302	1375		
145	1346	1284	1250	1220	1193	1190	1207	1244	1296	1370		
150	1348	1283	1238	1215	1186	1182	1200	1241	1295	1371		
155	1347	1280	1235	1205	1179	1173	1200	1237	1297	1371		
160	1345	1277	1230	1203	1176	1168	1197	1236	1299	1378	1536	1764
165	1346	1271	1229	1193	1172	1164	1196	1242	1297	1385	1562	1885
170	1348	1269	1228	1185	1167	1166	1196	1250	1306	1401	1577	1974
175	1349	1268	1227	1188	1166	1165	1196	1256	1320	1414	1599	2146
180	1350	1268	1224	1192	1169	1166	1203	1260	1333	1429	1634	2142
185	1348	1268	1222	1185	1173	1171	1208	1265	1347	1451	1670	2168
190	1347	1266	1220	1183	1170	1178	1216	1271	1347	1470	1704	2085
195	1342	1260	1220	1187	1172	1186	1222	1288	1363	1486	1716	2096
200	1339	1264	1218	1186	1180	1193	1232	1298	1376	1504	1727	2023
205	1345	1266	1216	1191	1188	1203	1241	1299	1384	1521	1738	2016
210	1349	1272	1227	1198	1194	1218	1254	1307	1398	1559	1781	2243
215	1352	1277	1239	1204	1207	1228	1262	1322	1406	1575	1866	2239
220	1354	1282	1246	1210	1218	1240	1274	1334	1422	1597	1951	2227
225	1356	1292	1254	1223	1230	1260	1301	1356	1456	1637	1989	2220
230	1359	1308	1264	1251	1244	1280	1331	1397	1484	1665	2008	2225
235	1363	1322	1278	1269	1263	1285	1340	1415	1497	1679	2051	2209
240	1371	1337	1296	1292	1283	1300	1348	1424	1537	1741	2105	2286
245	1379	1337	1317	1313	1300	1317	1360	1440	1583	1784	2195	2520
250	1385	1341	1346	1332	1318	1343	1382	1462	1638	1843	2353	2630
255	1392	1348	1366	1349	1342	1369	1422	1523	1766	2042	2454	2714
260	1396	1364	1388	1368	1368	1396	1454	1567	1921	2178	2324	2520
265				1388	1396	1426	1476	1581	1968	2056	2195	2369
270				1409	1433	1457	1505	1587	1889	2021	2120	2303
275				1439	1470	1499	1538	1616	1890	2012	2133	2346
280				1465	1499	1526	1560	1639	1897	1998	2177	2394
285				1499	1523	1560	1579	1656	1888	1996	2199	2426

TABLE V. (*Continued*).

Azimuth (deg.)	Zenith angle (deg)											
	5	10	15	20	25	30	35	40	45	50	55	60
290				1532	1560	1585	1611	1713	1895	2016	2195	2462
295	1360			1569	1591	1622	1656	1773	1916	2035	2218	2481
300	1354			1597	1636	1661	1711	1849	1957	2065	2254	2609
305	1348			1580	1661	1699	1767	1857	1958	2094	2282	2784
310	1345			1543	1642	1742	1797	1866	2002	2147	2293	2835
315	1341			1511	1599	1742	1808	1900	2046	2206	2452	2937
320	1337			1477	1549	1696	1773	1887	2115	2302	2773	2960
325	1334					1651	1700	1815	2213	2571	2833	2902
330	1333					1598	1643	1738	2217	2758	2840	2922
335	1334					1537	1587	1712	2386	2723	2892	3022
340	1334					1451	1519		2253	2692	2894	3038
345	1334					1385	1460		1970	2494	2823	2967
350	1335			1326	1322	1346	1408		1890	2486	2585	2881
355	1335			1313	1295	1320	1350		1685	2180	2417	2632

at 1 TeV. Our data provide new information on the flux of muons above 1 TeV.

VI. CONCLUSIONS

We measured the underground muon intensity as a function of the slant depth, in the range 3200–7000 hg cm^{-2}. The average parameters of the rock were estimated using the material extracted during the tunnel excavation and the mountain surveys (see the Appendix). The high statistics of this data sample allowed identification of regions where the mountain map is not well known. Our vertical muon intensities agree with the SOUDAN [18] and BAKSAN [6(g)] data and the world compilation of Ref. [17]; the Frejus [16] and the NUSEX [8] data are lower.

Using three different nuclear interaction models the primary "all-nucleon" spectrum has been evaluated in the energy range $2 < E_p < 200$ TeV/nucleon; it is compatible with the average of the available direct measurements in this energy range. The spectral index is almost model independent while the spread in the absolute normalization is about 25% larger than the statistical uncertainty.

From our data we determined the surface muon flux. For muon energies larger than 1 TeV, our data agree with the analytical estimate of Ref. [1].

APPENDIX: CHARACTERISTICS OF THE GRAN SASSO ROCK

The rock surrounding the Gran Sasso underground laboratory has an irregular structure; its composition is essentially calcareous, mixed with other materials, such as aluminum, silicon, magnesium compounds, and organic remains. Detailed analyses were made of the material obtained during the tunnel excavation. It was thus possible to make a composition and density model of the Gran Sasso rock [14]. The chemical composition is given in Table III.

The average values of the elemental composition parameters were calculated in the angular range 0°–60°; they are very close to the standard rock values (see Table IV). The correction to go from Gran Sasso to standard rock was applied following Ref. [13].

To evaluate the vertical muon intensity, the muon data were divided in angular bins $\Delta\theta = 1°$, $\Delta\phi = 2°$. For each bin a nominal rock thickness from the digitization of the mountain topographic map supplied by the Italian Military Geographical Institute (IGM) and a vertical muon intensity were evaluated. The distributions of the intensities for each angular bin exhibited, at fixed nominal depth, a Gaussian behavior. Some points are outside three standard deviations from the average as can be seen in Fig. 7 where the distribution in the quantity $[I((h,\theta,\phi) - \langle I(h,\theta,\phi)\rangle)/\sigma]$ is shown for three nominal depths. Figure 7 is an example of the study of the point to point uncertainties performed. In Fig. 7(b) the angular regions which yield muon intensities deviating more than $\pm 3\sigma$ from the average in the same slant depth are clearly visible. These regions have been identified and rejected. The data sample was reduced to 2.62×10^6 muons. In Table V the Gran Sasso rock thicknesses surviving the angular cuts previously described, are given as a function of the zenith and the azimuth angles. The azimuth is measured relative to geographic north. The empty bins represent the angular rejected regions according to the above criteria.

[1] T. Gaisser, *Cosmic Rays and Particle Physics* (Cambridge University Press, Cambridge, England, 1990).

[2] S.P. Ahlen *et al.*, Phys. Rev. D **46**, 895 (1992).

[3] S.P. Ahlen *et al.*, Phys. Rev. D **46**, 4836 (1992).

[4] M. Aglietta *et al.*, Phys. Lett. B **337**, 376 (1994).

[5] K. Asakimori *et al.*, in *Cosmic Ray Conference*, Proceedings of the 23rd International Conference, Calgary, Canada, 1993, edited by R. B. Hicks *et al.* (World Scientific, Singapore, 1994), Vol. 2, pp. 21 and 25; S. Swordy, *ibid.*, p. 243.

[6] (a) C. Castagnoli *et al.*, Nuovo Cimento A **82**, 78 (1984); (b) A. Castellina *et al.*, *ibid.* C **8**, 93 (1985); (c) L. Bergamasco *et al.*, *ibid.* **6**, 596 (1983); (d) P.H. Barrett *et al.*, Rev. Mod. Phys. **24**, 133 (1952); (e) L.M. Bollinger, Phys. Rev. **79**, 207 (1950); (f) R.I. Enikeev *et al.*, Sov. J. Nucl. Phys. **47**, 665 (1988); (g) Y.M. Andreyev, V.I. Gurentsov, and I.M. Kogai, in *Proceedings of the 20th International Cosmic Ray Conference*, Moscow, USSR, 1987, edited by V. Kozyarivsky *et al.* (Nauka, Moscow, 1987), Vol. HE 4.1-19; (h) V.N. Bakatanov *et al.*, Sov. J. Nucl. Phys. **55**, 1169 (1992).

[7] S.P. Ahlen *et al.*, Phys. Lett. B **249**, 149 (1990).

[8] M. Aglietta *et al.*, in *Astrophysics and Particle Physics*, Proceedings of the Topical Seminar, San Miniato, Italy, 1989, edited by G. Castellini *et al.* [Nucl. Phys. B (Proc. Suppl.) **14**, 193 (1990)].

[9] H. Adarkar *et al.*, in *Proceedings of the 21st International Cosmic Ray Conference*, Adelaide, Australia, 1989, edited by R. J. Protheroe (Graphic Services, Northfield, South Australia, 1990), Vol. 9, p. 310.

[10] S.P. Ahlen *et al.*, Nucl. Instrum. Methods A **234**, 337 (1993).

[11] S.P. Ahlen *et al.*, Astrophys. J. **412**, 301 (1993).

[12] R. Brun *et al.*, "CERN GEANT 3 User's Guide," Report No. DD/EE/84-1, 1992 (unpublished).

[13] Yu. D. Kotov and V. M. Logunov, in *Proceedings of the 11th International Cosmic Ray Conference*, Budapest, Hungary, 1969, edited by A. Somogyi [Acta Phys. Acad. Sci. Hung. Suppl. **29** (1970)].

[14] P.G. Catalano, "Caratteristiche geolitologiche e strutturali dell'ammasso roccioso sovrastante il laboratorio I.N.F.N.," ANAS report, 1986 (unpublished); P.G. Catalano *et al.*, Mem. Soc. Geol. It. **35**, 647 (1986).

[15] H. Bilokon *et al.*, "Muon survival probabilities in the Gran Sasso Rock," Report No. LNGS-94/92, 1994 (unpublished).

[16] Ch. Berger *et al.*, Phys. Rev. D **40**, 2163 (1989).

[17] M. Crouch, in *Proceedings of the 20th International Cosmic Ray Conference* [6], Vol. 6, p. 165.

[18] K. Ruddick (private communication); Soudan Collaboration, Int. Report No. PDK-435, 1990 (unpublished); S.M. Kasahara, Ph.D. thesis, University of Minnesota, 1995.

[19] C. Forti *et al.*, Phys. Rev. D **25**, 3668 (1990).

[20] R.S. Fletcher, T.K. Gaisser, P. Lipari, and T. Stanev, Phys. Rev. D **50**, 5710 (1994).

[21] L. Bergamasco *et al.*, Nuovo Cimento C **6**, 569 (1983).

[22] G. Parente, A. Shoup, and G.B. Yodh, Astropart. Phys. **3**, 17 (1995).

[23] MACRO Collaboration, M. Ambrosio *et al.*, in *Cosmic Ray Conference* [5], Vol. 2, p. 97.

[24] R.P. Kokoulin and A.A. Petrukin, in *Cosmic Ray Conference*, Proceedings of the 22nd International Conference, Dublin, 1991 (World Scientific, Singapore, 1991), Vol. 4, p. 536.

[25] P. Lipari and T. Stanev, Phys. Rev. D **44**, 3543 (1991).

[26] W. Lohmann, R. Kopp, and R. Voss, "Energy losses of muons in the energy range 1–10000 GeV," Report No. CERN 85-03, 1985 (unpublished).

[27] D.H. Perkins, Nucl. Phys. **B399**, 3 (1993).

[28] O.C. Allkofer, K. Carstensen, and W.D. Dau, Phys. Lett. **36B**, 425 (1971).

[29] C.A. Ayre *et al.*, J. Phys. G **1**, 584 (1975).

[30] P.J. Green *et al.*, Phys. Rev. D **20**, 1598 (1979).

[31] B.C. Nandi and M.S. Sinha, J. Phys. A **5**, 1384 (1972).

[32] B.C. Rastin, J. Phys. G **10**, 1609 (1984).